

# A Time Dependent Leptonic Model for Microquasar Jets: Application to LSI +61 303

S. Gupta and M. Böttcher

*Astrophysical Institute, Department of Physics and Astronomy, Clippinger Hall 251B, Ohio  
University, Athens, OH 45701 – 2979, USA*

## ABSTRACT

The Galactic high-mass X-ray binary and jet source (microquasar) LSI +61 303 has recently been detected at TeV  $\gamma$ -ray energies by the MAGIC telescope. We have applied a time-dependent leptonic jet model to the broadband spectral energy distribution and suggested (though not unambiguously detected) orbital modulation of the very high energy  $\gamma$ -ray emission of this source. Our model takes into account time dependent electron injection and acceleration, and the adiabatic and radiative cooling of non-thermal electrons. It includes synchrotron, synchrotron self-Compton and external inverse Compton (with seed photons from the companion star), as well as  $\gamma\gamma$  absorption of  $\gamma$ -rays by starlight photons. The model can successfully reproduce the available multiwavelength observational data. Our best fit to the SED indicates that a magnetic field of  $B_0 \sim 5 \times 10^3$  G at  $\sim 10^3 R_g$  is required, and electrons need to be accelerated out to TeV energies ( $\gamma_2 = 10^6$ ) with a nonthermal injection spectrum with a spectral index of  $q = 1.7$ , indicating the operation of acceleration mechanisms beyond the standard first-order Fermi mechanism at relativistic or non-relativistic shocks. The orbital modulation of the VHE  $\gamma$ -ray emission can be explained solely by the geometrical effect of changes in the relative orientation of the stellar companion with respect to the compact object and jet as it impacts the position and depth of the  $\gamma\gamma$  absorption trough. Such a scenario predicts a trend of spectral hardening during VHE  $\gamma$ -ray low orbital phases.

*Subject headings:* radiation mechanisms: non-thermal — gamma-rays: theory — X-rays: binaries

## 1. Introduction

X-ray binaries with relativistic jets, or microquasars, have recently been established as a new class of  $\gamma$ -ray emitting sources. Two sources detected by EGRET on board the *Compton Gamma-Ray Observatory* were found to be spatially consistent with the locations of microquasars, namely LS 5039 and LSI +61 303 (Hartman et al. 1999). Observations of  $\gtrsim 250$  GeV  $\gamma$ -rays from LS 5039 with the High Energy Stereoscopic System (HESS) have recently shown this high-mass source to be a TeV emitter (Aharonian et al. 2005), also strengthening its earlier tentative identification with the EGRET source 3EG J1824-1514 (Paredes et al. 2000). The second source, LSI +61 303, associated with the COS-B source 2CG 135+01 (Hermsen et al. 1977; Gregory & Taylor 1978) and the EGRET source 3EG J0241+6103 (Kniffen et al. 1997), was recently observed with the Major Atmospheric Gamma-ray Imaging Cherenkov (MAGIC) telescope by Albert et al. (2006). They detected variable  $\gamma$ -ray emission above 100 GeV over six orbital cycles, suggesting a periodic modulation on the time scale of the orbital period of 29.496 d, though further observations are necessary to firmly establish the correlation between the VHE variability and the orbital period. The strongest detections were not at the periastron, suggesting that the modulation might not be related to a modulation of the accretion rate (as suggested by, e.g., Romero et al. 2003; Bosch-Ramon & Paredes 2004b), but rather to geometrical effects. Geometrical effects causing an orbital modulation of the high-energy emission include the azimuthal-angle dependence of the  $\gamma\gamma$  absorption of high-energy emission by starlight photons (Böttcher & Dermer 2005; Dubus 2006) or of the Compton upscattering of starlight photons by relativistic electrons in the microquasar jet (Dermer & Böttcher 2006). Dubus (2006) has performed a detailed analysis of the  $\gamma\gamma$  absorption of VHE photons in the photon field of the stellar companion, taking into account the finite size of the star and the eccentricity of the orbit for the case of VHE emission from the surface of a putative neutron star associated with LSI +61 303. Note that he used a definition of the phase such that phase 0 corresponds to the periastron passage, so that his results should be shifted by  $\Delta\psi = 0.23$  (see below) when compared to the definition commonly used throughout the literature on this object, including this *Letter*. He found that the  $\gamma\gamma$  absorption depth is expected to show a pronounced maximum at phases just before the periastron passage, when the compact object is located behind the stellar companion. The recent VHE detections, along with the observation of X-ray jet structures in several microquasars using *Chandra* and *XMM-Newton* (Corbel et al. 2002; Tomsick 2002, e.g.), have re-ignited interest in jet models for the high energy emission from microquasars, analogous to the commonly adopted models for blazars (for a recent review see, e.g. Böttcher 2002).

In the leptonic model of microquasars, Very High Energy (VHE) emission might most likely originate near the base of the mildly relativistic jet. The soft photons from the companion star, the accretion disk as well as from jet synchrotron radiation can be Compton

upscattered by the ultra-relativistic electrons in the jet. Steady-state leptonic jet models of the  $\gamma$ -ray emission from microquasars have been presented, e.g., by Bosch-Ramon & Paredes (2004a,b), and (Dermer & Böttcher 2006). A time-dependent, broadband leptonic jet model was presented in Gupta et al. (2006), (henceforth, Paper 1) where an analytical solution to the electron kinetic equation was presented, restricting the analysis to Compton scattering in the Thomson regime. This *Letter* follows up on the analysis of Paper 1, now incorporating a full Klein-Nishina treatment of the Compton scattering as well as the angle dependence of the stellar radiation field. We then apply the new model to broadband observations of LSI +61 303, including the effect of the orbital modulation on the  $\gamma\gamma$  absorption in the  $>100\text{GeV}$  range. In §2, we present a general outline of the model geometry and the radiative processes involved. §3 shows the application to LSI +61 303, and we conclude with a brief summary in §4.

## 2. Model Description

The accretion flow onto the central compact object is ejecting a twin pair of jets, assumed to be oriented perpendicular to the orbital plane, which is inclined with respect to the line of sight by an angle  $i$ . Two intrinsically identical disturbances, containing non-thermal plasma (blobs) originate from the central source at the same time, traveling in opposite directions along the jet at a constant speed  $v_j = \beta_j c$ . Over a limited range in distance  $x_0 \leq x \leq x_1$ , relativistic electrons are accelerated and injected in the emission region with an exponentially cut-off power-law distribution in electron energies ( $E_e = \gamma m_e c^2$ ) with low- and high-energy cutoffs  $\gamma_1$  and  $\gamma_2$ , respectively, in the co-moving frame:

$$Q_e^{\text{inj}}(\gamma; t) = Q_0^{\text{inj}}(t) \gamma^{-q} e^{-\gamma/\gamma_2}, \quad \gamma_1 \leq \gamma. \quad (1)$$

The normalization factor  $Q_e^{\text{inj}}$  is approximately related to the power injected into relativistic electrons,  $L_{\text{inj}}$  through

$$Q_0 \approx \begin{cases} \frac{L_{\text{inj}}(2-q)}{m_e c^2 (\gamma_{\text{max}}^{2-q} - \gamma_{\text{min}}^{2-q})} & \text{if } q \neq 2; \\ \frac{L_{\text{inj}}}{m_e c^2 \ln(\gamma_{\text{max}}/\gamma_{\text{min}})} & \text{if } q = 2. \end{cases} \quad (2)$$

The injection luminosity  $L_{\text{inj}}$  and the functional dependence of Eq. (1) are held constant between  $x_0$  and  $x_1$ . The blob's (transverse) radius,  $R_{\perp}$ , scales with distance from the central engine as  $R_{\perp} = R_{\perp}^0 (x/x_0)^{\alpha}$ , i.e.,  $\alpha = 0$  corresponds to perfect collimation, and  $\alpha = 1$  describes a conical jet. Following the arguments given in Atoyan & Aharonian (1997),

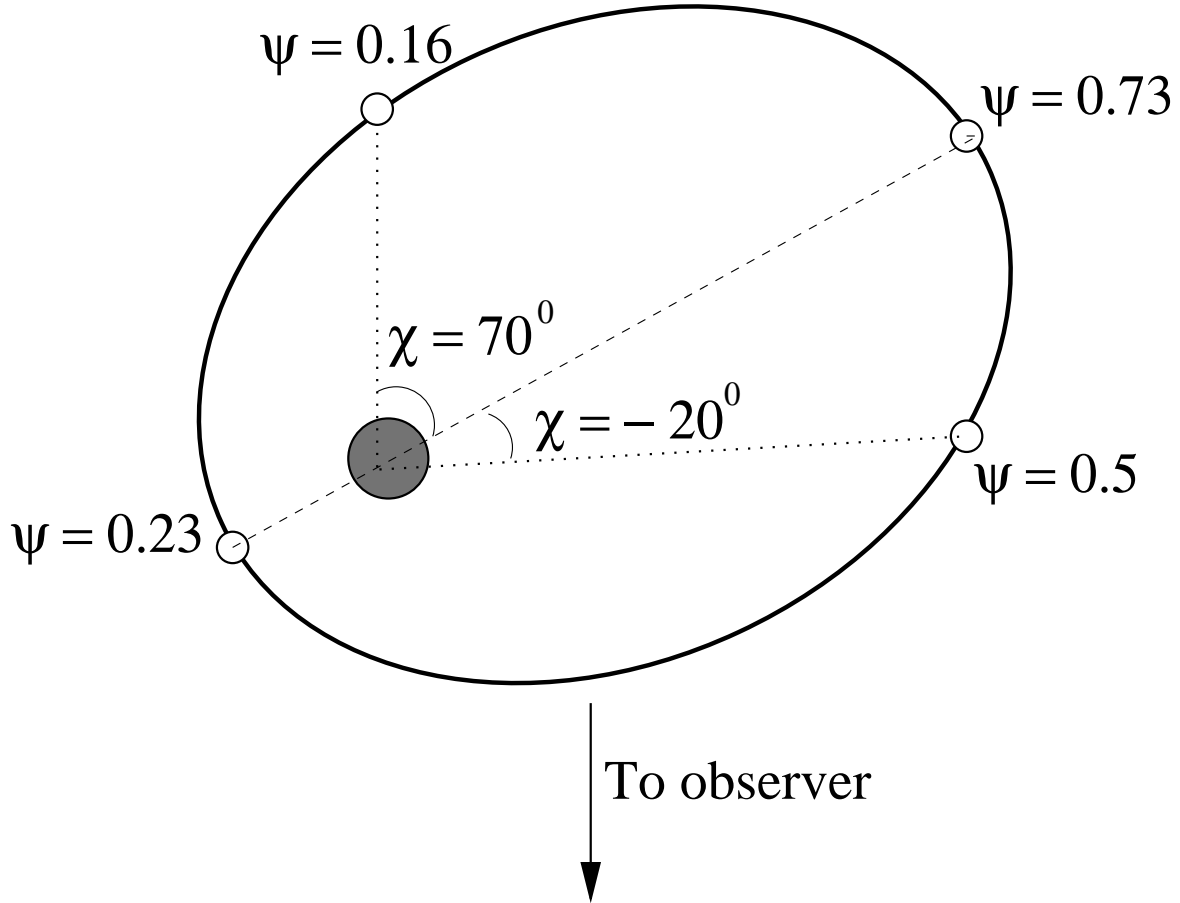


Fig. 1.— Sketch of the geometry of the binary orbit of LSI +61 303, approximating the massive (Be) star to be stationary. The labels on the compact-object orbit indicate the orbital phase  $\psi$  as well as the azimuthal angle with respect to the apastron,  $\chi$ .

we choose a magnetic-field dependence on distance from the central black hole as  $B(x) = B_0 (R_\perp/R_\perp^0)^{-2} = B_0 (x/x_0)^{-2\alpha}$ .

The geometry of the orbit of the LSI +61 303 system is illustrated in Fig. 1. In order to incorporate the orbital modulation of the Compton scattering, we replaced the circular orbit of the binary system in Paper 1 by an elliptical one, so that the distance of the star to the compact object now varies as

$$r(\chi) = \frac{a(1 - e^2)}{1 - e \cos(\chi)} \quad (3)$$

where  $a$  is the semi-major axis,  $e$  is the eccentricity of the orbit, and  $\chi$  is the phase angle (which is *not* linearly related to the orbital phase  $\psi$ , in contrast to the incorrect expression

in Romero et al. 2005). The  $\gamma\gamma$  opacity as a function of  $\gamma$ -ray photon energy and orbital phase has been calculated following Böttcher & Dermer (2005).

To treat the time-dependent electron dynamics and the radiation transfer in the emitting blob, we solve the continuity equation for the relativistic electrons,

$$\frac{\partial n_e(\gamma, t)}{\partial t} = -\frac{\partial}{\partial \gamma} \left[ \left( \frac{d\gamma}{dt} \right)_{loss} n_e(\gamma, t) \right] + Q_e^{inj}(\gamma, t) \quad (4)$$

where,  $(d\gamma/dt)_{loss}$  is the (radiative and adiabatic) energy loss rate for the electrons. The electron cooling rates are calculated using subroutines used in the jet radiation transfer code of Böttcher, Mause & Schlickeiser (1997) and Böttcher & Bloom (2000). The discretized electron continuity equation can be written in the form of a tridiagonal matrix (Chiaberge & Ghisellini 1999), and solved using the standard routine of Press et al. (1992).

Radiation mechanisms included in our simulations are synchrotron emission, Compton upscattering of synchrotron photons, namely synchrotron self-Compton (SSC) emission, and Compton upscattering of external photons. The dominant external soft photon source is the companion star (for details, refer to Paper 1) which is approximated as a point source, emitting a blackbody with dimensionless temperature  $\Theta_* = kT_*/m_e c^2$ .

### 3. Application to LSI +61 303

#### 3.1. Parameter Selection

The high mass XRB, LSI +61 303, at a distance of 2 kpc (Hutchings & Crampton 1981; Frail & Hjellming 1991) has been observed from radio (Paredes et al. 1996) to TeV  $\gamma$ -rays (Albert et al. 2006), providing a wealth of broadband data to test various emission models. However, most of the models until now dealt more with the radio, X-ray, or  $\gamma$ -ray variability of the source, than with its broadband properties and its very-high-energy emission. Recently, however, Chernyakova et al. (2006) reproduced the broadband spectrum of the system, including the recent MAGIC detection, using a model of a rotation powered pulsar. The (slight) orbital modulation of the X-ray and  $\gamma$ -ray emission in the *XMM-Newton* and *INTEGRAL* energy ranges was explained based on a variable injection rate of high energy electrons. The VHE  $\gamma$ -ray emission was attributed to hadronic processes, initiated by high-energy protons in the pulsar wind, and its orbital modulation was not explained in that model. In contrast, in this *Letter*, we are specifically addressing the broadband spectral characteristics *and* the orbital modulation of the VHE  $\gamma$ -ray emission.

Casares et al. (2005) have found a mass function of  $f(M) \approx 0.011 M_\odot$ . Since the inclination angle  $i$  between the line of sight and the normal to the orbital plane (which, in our model is identical to the jet axis) is poorly constrained, and also the mass of the B0 V type stellar companion (with a dense equatorial wind) is not well known and in the range of  $M_* \sim 10 - 15 M_\odot$ , a rather wide range of masses for the compact object is consistent with the observational constraints, even including a  $1.4 M_\odot$  neutron star (Hutchings & Crampton 1981). In our model, we follow the suggestion of Casares et al. (2005) of  $i = 30^\circ$  and adopt a companion mass of  $\sim 12 M_\odot$ , which would yield  $M_X \sim 2.67 M_\odot$ . The orbit has an eccentricity of  $e = 0.72 \pm 0.15$ , the orbital period is  $\sim 26.496$  d (Gregory 2002), and the orbital semi major axis is  $a = 5 \times 10^{12}$  cm. MERLIN observations by Massi et al. (2004) imply a jet Lorentz factor of  $\Gamma_{jet} = 1.25$ .

In our fitting procedure, we are varying the following parameters: the low and high energy cut-off of the electron injection spectrum  $\gamma_1$  and  $\gamma_2$ , respectively, the injection spectral index  $q$ , the initial distance of the injection zone from the compact object  $x_0$ , and the initial magnetic field  $B_0$ . The straight power-law shape of the X-ray spectrum indicates that any disk blackbody component from an accretion disk around the compact object should have a luminosity of  $L_D \lesssim 10^{34}$  ergs  $s^{-1}$  and be at least  $\sim 4$  orders of magnitude lower than the luminosity of the companion star. For such low disk luminosities, external Compton scattering of accretion disk photons will be negligible as well. The evolution of the electron distribution in the emitting region is followed over a period of  $\sim 5$  days ( $\ll P_{orb}$ ). Since most of the high-energy emission emanates from the system within the first few seconds of electron evolution, the orbital phase is taken to be a constant for each run of our model. Also, the centre of mass of the system lies close to the massive ( $12 M_\odot$ ) stellar companion, so that the compact object essentially orbits the stellar companion, which is assumed to be stationary.

For an initial spectral fit, we concentrate on the orbital phase during which MAGIC significantly detected the source. Specifically, we chose  $\psi = 0.5$ , corresponding to a phase angle  $\chi = -20^\circ$ . This resulted in a best fit for which all physical parameters are summarized in Table 1.

### 3.2. Results

In Fig. 2, we show the computed SEDs of LSI +61 303 using the parameters listed in Table 1. The black solid line corresponds to our best fit to the SED at the orbital phase of  $\psi = 0.5$  ( $\chi = -20^\circ$ ). The figure also shows the individual contributions of the synchrotron, stellar, and SSC emission, as well as the inverse Compton (EC) scattering of

starlight photons.

The overall agreement of the simulated SED at  $\psi = 0.5$  with the observed spectrum is very good, given that the multiwavelength data is not simultaneous. Since the radio emission most likely originates from regions of the jet further away from the compact object than the evolution modeled here, our model underpredicts the VLA data (not included in the figure). The NIR data (Strickman et al. 1998) has been de-reddened using  $N_H = 8.4 \times 10^{21} \text{ cm}^{-2}$  (Taylor et al. 1996). The infrared emission might be dominated by emission from the outer parts of the circumstellar disk around the Be star which is not included in our model.

In order to reproduce the keV – MeV data, a magnetic field of  $5 \times 10^3 \text{ G}$  is required at a distance of  $\sim 1.7 \times 10^9 \text{ cm}$  from the compact object. In the X-ray band, most of the radiation is synchrotron emission from the jet (also see, e.g. Paredes et al. 2006), with negligible contributions from SSC or EC. The SSC contribution dominates the spectrum at TeV energies. Note that the individual SSC component in Fig. 2 does not include the  $\gamma\gamma$  absorption feature, which is only applied to the total emanating spectrum.

After our fit to the  $\psi = 0.5$  phase spectrum, we performed a model simulation with the same intrinsic jet parameters, but changed the orbital geometry to  $\psi = 0.16$  ( $\chi = 70^\circ$ ), corresponding to the MAGIC low state. Since the EC (star) component was rather insignificant, this will impact essentially only the  $\gamma\gamma$  absorption. The corresponding model fit is illustrated by the solid red line in Fig. 2. In this case, the  $\gamma\gamma$  absorption trough is deeper because (a) VHE  $\gamma$ -rays pass by the star more closely than their nearest approach in the  $\psi = 0.5$  geometry, and (b) starlight photons intercept VHE photons at a more favorable angle for  $\gamma\gamma$  absorption, leading to a lower energy threshold for this process. In this phase, our model predicts an integrated flux over 400 GeV of  $F(E > 400\text{GeV}) \approx 2.2 \times 10^{-12} \text{ ph cm}^{-2} \text{ s}^{-1}$ . This is in perfect agreement with the  $2\sigma$  upper limit of  $F(E > 400\text{GeV}) < 3 \times 10^{-12} \text{ ph cm}^{-2} \text{ s}^{-1}$  given in Albert et al. (2006) and indicated by the maroon arrow in Fig. 2. Consequently, we find that the orbital modulation of the VHE emission in LS +61 303 can be explained solely by the effect of the azimuthal asymmetry of  $\gamma\gamma$  absorption feature due to starlight photons.

#### 4. Summary and Conclusions

We have applied a leptonic jet model to the broadband spectral energy distribution and orbital modulation of the VHE  $\gamma$ -ray emission of the microquasar LSI +61 303, taking into account time dependent electron injection and acceleration, and the adiabatic and radiative cooling of non-thermal electrons. Our model includes synchrotron, synchrotron self-Compton and external inverse Compton emission (with seed photons predominantly from the compan-

ion star), as well as  $\gamma\gamma$  absorption of  $\gamma$ -rays by starlight photons. Compton scattering is treated using the full Klein Nishina cross section and the full angular dependence of the stellar radiation field.

The model can successfully reproduce the available multiwavelength observational data, including the most recent MAGIC detection in the TeV range (Albert et al. 2006). Our best fit to the SED indicates that a magnetic field of  $B_0 \sim 5 \times 10^3$  G at  $\sim 10^3 R_g$  is required, and electrons need to be accelerated out to TeV energies ( $\gamma_2 = 10^6$ ) with a nonthermal injection spectrum with a spectral index of  $q = 1.7$ . Such an injection spectrum can not be achieved by the first-order Fermi mechanism at relativistic or non-relativistic shocks (e.g., Gallant et al. 1999; Achterberg et al. 2001) and therefore suggests that 2<sup>nd</sup> order Fermi acceleration (Virtanen & Vainio 2005) and/or acceleration at shear boundary layers (Ostrowski 2000; Stawarz & Ostrowski 2002; Rieger & Duffy 2004) may play a significant role in the acceleration of relativistic particles in microquasar jets. In our model, the X-ray and  $\lesssim 1$  GeV  $\gamma$ -ray emission is dominated by synchrotron emission from the jet, while SSC emission dominates the VHE  $\gamma$ -ray emission.

The suggested orbital modulation of the VHE  $\gamma$ -ray emission can be explained solely by the geometrical effect of changes in the relative orientation of the stellar companion with respect to the compact object and jet as it impacts the position and depth of the  $\gamma\gamma$  absorption trough (Böttcher & Dermer 2005). If this interpretation is correct, a general trend of spectral hardening at TeV energies during VHE  $\gamma$ -ray low phases is predicted. Although additional effects of a varying accretion rate due to the highly eccentric orbit of the binary system are likely to occur, they are not necessary to explain the observed orbital modulation of the VHE emission of LSI +61 303.

We thank the anonymous referee for useful comments and a quick review, and C. D. Dermer, G. Dubus, and V. Bosch-Ramon for helpful comments and discussions. This work was partially supported by NASA through INTEGRAL GO (Theory) grant award no. NNG 05GK59G.

## REFERENCES

- Achterberg, A., et al., 2001, MNRAS, 328, 393  
 Aharonian F., et al., 2005, Science, 309, 746  
 Albert, J., et al., 2006, Science, Vol. 312, Issue 5781, p. 1771

- Atoyan, A. M., & Aharonian, F. A., 1997, *ApJ*, 490, L149
- Böttcher, M., 2002, in proc. “The Gamma-Ray Universe”, XXII Moriond Astrophysics Meeting, eds. A. Goldwurm, D. N. Neuman, & J. T. T. Vãn, p. 151
- Böttcher, M., & Bloom, S. D., 2000, *AJ*, 119,469
- Böttcher, M., & Dermer, C. D., 2005, *ApJL*, 634L, 81B
- Böttcher, M., Mause, H., & Schlikeiser, R.,1997, *A&A*,324,395
- Bosch-Ramon, V., & Paredes, J. M., 2004a, *A&A*, 417, 1075
- Bosch-Ramon, V., & Paredes, J. M., 2004a, *A&A*, 425 1069
- Casares, J., Ribas, I., Paredes, J. M., Martí, J., and Allende Prieto, C., 2005, *MNRAS*, 360, 1105
- Chernyakova, M., Neronov, A., & Walter, R., 2006, *MNRAS*, submitted (astro-ph/0606070)
- Chiaberge, M., & Ghisellini, G., 1999, *MNRAS*, 306, 551
- Corbel, S., Fender, R. P., Tzioumis, T., Tomsick, J. A., Orosz, J. A., Miller, j. M., Wijnands, R., & Kaaret, P., 2002, *Science*, 298, 196
- Dermer, C. D., & Böttcher, M., 2006, *ApJ*, 643, 1081
- Dubus, G., 2006, *A&A*, 451, 9
- Rieger, F. M., & Duffy, P., 2004, *ApJ*, 617, 155
- Frail, D. A., & Hjellming, R. M.,1991, *AJ*,101,2126
- Gallant, Y., et al., 1999, *A&AS*, 138, 549
- Goldoni, P., & Mereghetti, S., 1995, *A&A*, 299, 751
- Gregory, P. C.,2002, *ApJ*, 575, 427
- Gregory, P. C., & Taylor, A. R., 1978, *Nature*, 272, 704
- Gupta, S., Böttcher, M., & Dermer, C. D., 2006, *ApJ*, 644, 409
- Harrison, F. A., Ray, P. S., Leahy, D. A., Waltman, E. B., & Pooley, G. G., 2000, *ApJ*, 528, 454

- Hartman, R. C., 1999, *ApJS*, 123, 79
- Hermesen, W., et al., 1977, *Nature*, 269, 494
- Hutchings, J. B., & Crampton, D., 1981, *PASP*, 93, 486
- Kniffen, D. A., et al., 1997, *ApJ*, 486, 126
- Leahy, D., 2003, in proc. of 28<sup>th</sup> ICRC, Tsukuba, Japan, 2003; Univ. Academy Press, Inc.; p. 2461
- Massi, M., Ribò, M., & Paredes, J. M., 2004, *A&A*, 414, L1
- Ostrowski, M., 2000, *MNRAS*, 312, 579
- Paredes, J. M., et al., 1996, *ASPC*, 93, 243P
- Paredes, J. M., Martí, J., Ribò, M., & Massi, M., 2000, *Science*, 288, 2340
- Paredes, J. M., Bosch-Ramon, V., & Romero, G. E., 2006, *A&A*, 451, 259
- Press, W. H., et al., 1992, *Numerical Recipes in C* (Cambridge: Cambridge Univ. Press)
- Romero, G. E., Torres, D. F., Kaufman Bernardó, M. M., Mirabel, I. F., *A&A*, 410, L1
- Romero, G. E., Christiansen, H. R., & Orellana, M., 2005, *ApJ*, 632, 1093
- Stawarz, L., & Ostrowski, M., 2002, *ApJ*, 578, 763
- Strickman, M. S., et al., 1998, *ApJ*, 497, 419
- Taylor, A. R., Young, G., Peracaula, M., Kenny, H. T., & Gregory, P. C., 1996, *A&A*, 305, 817
- Tomsick, J. A., Corbel, S., Fender, R. P., Miller, J. M., Orosz, J. A., Tzioumis, T., Wijnands, R., & Kaaret, P., 2002, *ApJ*, 582, 933
- Virtanen, J. J. P., & Vainio, R., 2005, *ApJ*, 621, 313

Table 1. Relevant parameter choices for our best fit to the broadband spectrum of LSI +61 303

Parameter	Symbol	Value
Distance	$d$	$6.17 \times 10^{21}$ cm
Jet inclination angle	$i$	$30^\circ$
Bulk Lorentz factor	$\Gamma_j$	1.25
Semi Major Axis	$a$	$5 \times 10^{12}$ cm
Luminosity of companion star:	$L_*$	$2 \times 10^{38}$ ergs s $^{-1}$
Surface temperature of the companion star	$T_*$	$2.25 \times 10^4$ K
Initial blob radius	$R_0$	$10^3 R_g$
Jet collimation parameter	$\alpha$	0.3
Electron injection spectrum, low-energy cutoff	$\gamma_{\min}$	10
Electron injection spectrum, high-energy cutoff	$\gamma_{\max}$	$10^6$
Electron injection spectrum, spectral index	$q$	1.7
Beginning of electron injection zone	$x_0$	$10^3 R_g$
End of electron injection zone	$x_1$	$10^5 R_g$
Magnetic field at $x_0$	$B_0$	$5 \times 10^3$ G
Injection luminosity	$L_{\text{inj}}$	$10^{35}$ ergs s $^{-1}$
Orbital Period	$P$	26.496 days
Orbit eccentricity	$e$	0.72

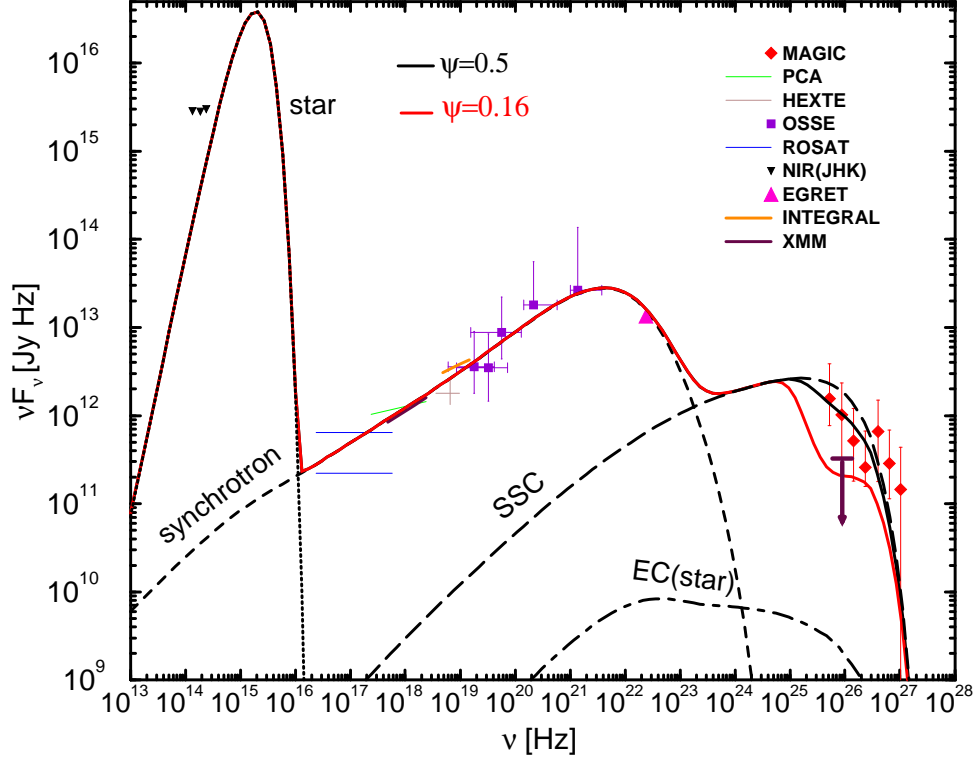


Fig. 2.— Spectral energy distribution of LSI +61 303. The plotted observational data corresponds to  $\psi \sim 0.5$  and are taken from: Albert et al. (2006) (MAGIC), Harrison et al. (2000) (RXTE PCA + HEXTE), Strickman et al. (1998) (OSSE, NIR), Goldoni & Mereghetti (1995) (ROSAT), Leahy (2003) (EGRET), Chernyakova et al. (2006) (XMM, INTEGRAL). Also included is the MAGIC  $2\sigma$  upper limit for phase  $\psi \sim 0.2$  (Albert et al. 2006). The solid curves show our fit results with  $\gamma\gamma$  absorption calculated for  $\psi \sim 0.5$  (black) and  $\psi \sim 0.16$  (red). A trend of spectral hardening at TeV energies during VHE low phases is predicted.